NOAA Technical Memorandum EDS BOMAP-13

WATER-VAPOR AND MASS DIVERGENCE COMPUTATIONS BASED ON BOMEX AIRCRAFT AND RAWINSONDE DATA: A COMPARISON

Robert W. Reeves

Center for Experiment Design and Data Analysis
Washington, D.C.
December 1974

noaa NATIONAL OCEANIC AND ATMOSPHERIC ADMINISTRATION / Environmental Data Service

NOAA TECHNICAL MEMORANDA

Environmental Data Service, BOMAP Series

The Barbados Oceanographic and Meteorological Experiment (BOMEX) was conducted in May, June, and July 1969. Following the field experiment, the Barbados Oceanographic and Meteorological Analysis Project (BOMAP) was established in the Research Laboratories (ESSA), now NOAA, to coordinate the reduction of the data collected; to analyze these data, particularly those pertaining to the Sea-Air Interaction Program (the BOMEX Core Experiment); and to provide a central contact point for information exchange and publication of BOMEX results.

The name of the BOMAP Office was subsequently changed to Center for Experiment Design and Data Analysis (CEDDA), which was transferred to NOAA's Environmental Data Service in 1972. BOMAP remains, however, one of CEDDA's responsibilities, and publication of NOAA Technical Memoranda will continue as a means for disseminating information resulting from analyses of BOMEX data conducted at CEDDA. ERLTM-BOMAP-1 was published in the series of ESSA Technical Memoranda, ESSA Research Laboratories. ERL BOMAP-2 through ERL BOMAP-9 were issued as part of the series of NOAA Technical Memoranda, Environmental Research Laboratories. Subsequent publications are part of the series of NOAA Technical Memoranda, Environmental Data Service.

Publications listed below are available from the National Technical Information Service, U.S. Department of Commerce, Sills Bldg., 5285 Port Royal Road, Springfield, Va. 22151. Price: Paper copy prices vary; $1.45 for microfiche. Order by accession number shown in parentheses at end of each entry.

ESSA Technical Memoranda

ERLTM-BOMAP 1 High-Level Cloud Photography Inventory, BOMEX Period IV, July 11-28, 1969. Vance A. Myers, September 1970, 66 p. (PB-194-661)

NOAA Technical Memoranda

ERL BOMAP-2 A Statistical Data Plan for BOMEX. Theodore W. Horner, December 1970, 105 p. (COM-71-00188)

ERL BOMAP-3 Mass, Momentum, and Energy Budget Equations for BOMAP Computations. Eugene M. Rasmusson, January 1971, 32 p. (COM-71-00195)

ERL BOMAP-4 High-Level Cloud Photography Inventory, BOMEX Period II, May 24-June 10, 1969. Vance A. Myers, March 1971, 86 p. (COM-71-00574)

ERL BOMAP-5 Preliminary Velocity Divergence Computations for BOMEX Volume Based on Aircraft Winds. Robert W. Reeves, April 1971, 21 p. (COM-71-00667)

ERL BOMAP-6 Ship's Influence on Surface and Rawinsonde Temperatures During BOMEX. Warren M. Wisner, June 1971, 44 p. (COM-71-00950)

ERL BOMAP-7 High-Level Cloud Photography Inventory, BOMEX Period I, May 3-15, 1969. Vance A. Myers, December 1971, 55 p. (COM-72-10196)

ERL BOMAP-8 BOMEX Flight Tracks Reconstructed From Near-Simultaneous High-Level Cloud Photography by Two Aircraft. Vance A. Myers and Martin Predoehl, December 1971, 13 p. (COM-72-10313)

ERL BOMAP-9 The BOMEX Sea-Air Interaction Program: Background and Results to Date. Joshua Z. Holland, March 1972, 34 p. (COM-72-10576)

EDS BOMAP-10 BOMEX Rainy Day Analysis. Lt. Garry W. Elliott, July 1973, 9 p. (COM-74-10466)

EDS BOMAP-11 Method for Obtaining Wet-Bulb Temperatures by Modifying the Psychrometric Formula. J. Sullivan and L. D. Sanders, June 1974. (COM-74-11425/AS)

EDS BOMAP-12 Profiles in the Lowest 300 Meters of the Marine Tropical Planetary Boundary Layer. C. F. Ropelewski, September 1974, 24 pp. (COM-74-11779/AS)

NOAA Technical Memorandum EDS BOMAP-13

WATER-VAPOR AND MASS DIVERGENCE COMPUTATIONS BASED ON BOMEX AIRCRAFT AND RAWINSONDE DATA: A COMPARISON

Robert W. Reeves

Center for Experiment Design and Data Analysis
Washington, D.C.
December 1974

UNITED STATES
DEPARTMENT OF COMMERCE
Frederick B. Dent, Secretary

NATIONAL OCEANIC AND
ATMOSPHERIC ADMINISTRATION
Robert M. White, Administrator

Environmental Data
Service
Thomas S. Austin, Director

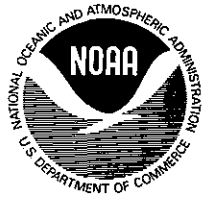

CONTENTS

WATER-VAPOR AND MASS DIVERGENCE COMPUTATIONS BASED ON BOMEX AIRCRAFT AND RAWINSONDE DATA: A COMPARISON

Robert W. Reeves
Center for Experiment Design and Data Analysis
National Oceanic and Atmospheric Administration
Washington, D.C. 20235

Abstract. Water-vapor and mass divergences were computed from aircraft and rawinsonde data collected during the Barbados Oceanographic and Meteorological Experiment (BOMEX) in 1969. The contribution to the water-vapor flux divergence by horizontal subgrid-scale eddies was found to be unimportant during undisturbed weather conditions. Correlation coefficients and rms differences between measurements of the same horizontal wind derivatives by different systems are discussed. Results indicate that divergence computations based on data from a single four-aircraft mission are comparable in accuracy to those based on rawinsonde data averaged over four release times and 50 mb.

1. INTRODUCTION

The Barbados Oceanographic and Meteorological Experiment (BOMEX) was conducted in the summer of 1969. Built into the design of the BOMEX sea-air interaction program, or Core Experiment, whose objectives have been described by Holland (1970), were redundant measurements of many parameters necessary for atmospheric budget computations. Derivations of the budget equations for the volume overlying the 500-km by 500-km BOMEX square array have been discussed in detail by Rasmusson (1971), and a trial analysis of the atmospheric budgets of mass, water vapor, heat, momentum, and mechanical energy has been presented by Holland and Rasmusson (1973). The latter analysis was based on rawinsonde data obtained during a 5-day period of intensive data gathering from June 22 through 26. In computing divergence values for the mass budget, they compared results obtained from the rawinsonde observations with values based on aircraft data collected on three missions during the same period and found close agreement at levels below the trade-wind inversion.

Fleagle et al. (1967) computed water-vapor fluxes over the Indian Ocean by line integral techniques based on aircraft data and compared these with fluxes computed from profiles on an instrumented buoy. However, they found that measurements by a single aircraft flying along the perimeter of an area are sometimes inadequate for budget computations because changes in the variables measured occur in the course of any single mission. They therefore recommended use of aircraft on opposite sides of an area.

In view of these findings, a closer examination seemed desirable to further test the feasibility of using aircraft data in budget computations. In this paper such an examination is made by various intercomparisons of BOMEX aircraft and rawinsonde data.

2. DATA BASE

Data collected from June 22 through June 30 were selected for this study because of the operational success of the rawinsonde and aircraft programs during this period.

2.1 Aircraft Data

The aircraft data were gathered on five multiple-level line integral missions: three flown during the day on June 22, 29, and 30, and two at night on June 23-24 and June 25-26, 1969 (BOMAP Office, 1971). Four aircraft participated in each mission, operating in pairs. One pair flew in formation at an altitude of 300 m from Barbados to the midpoint of the south side of the array, then parted, with one aircraft operating on the west side and the other on the east side of the BOMEX square, each flying four traverses at levels of 300, 1,300, and 2,300 m and, again, 300 m. The second pair of aircraft, parting at the midpoint of the west side of the array, operated in the same way to cover the north and south sides of the BOMEX square (fig. 1). "Calibration boxes" were flown by each aircraft at the end of each leg and at each level for measurement of systematic errors in drift angle and airspeed data. Total flight time for each aircraft, including the inbound and outbound intercomparison legs, for one mission was 12 hr, but each 500-km flight leg at the four levels was covered in 1 1/2 hr.

Two aircraft from NOAA's Research Flight Facility (RFF) were always used on the east and west sides of the array and two Navy aircraft, or one RFF and one Navy aircraft, on the north and south sides. The RFF aircraft had rapid automatic recording systems that sampled the atmosphere every second. By contrast, on the Navy aircraft, a set of 10 rapid readings of drift angle, airspeed, groundspeed, and heading was tabulated manually every 5 min on the flight legs, and 5 rapid readings were taken on all headings flown during calibration maneuvers. For purposes of this study, each set was averaged to produce a single observation every 5 min, yielding approximately 15 data points for each flight along one side of the array.

Winds were computed from readings of heading, drift angle, true airspeed, and groundspeed. Errors in the last three were partly removed after the flight by using calibration box data (Reeves, 1971). The remaining differences in the aircraft crosstrack winds were reconciled by calculating the average difference based on the data for the outbound and inbound intercomparison legs, and using this information to correct one wind measurement on one of the aircraft for an entire mission. Since the crosstrack winds are critically dependent on the drift-angle measurements, and since drift-angle errors are not dependent on height, applying the correction at all flight levels seemed justified.

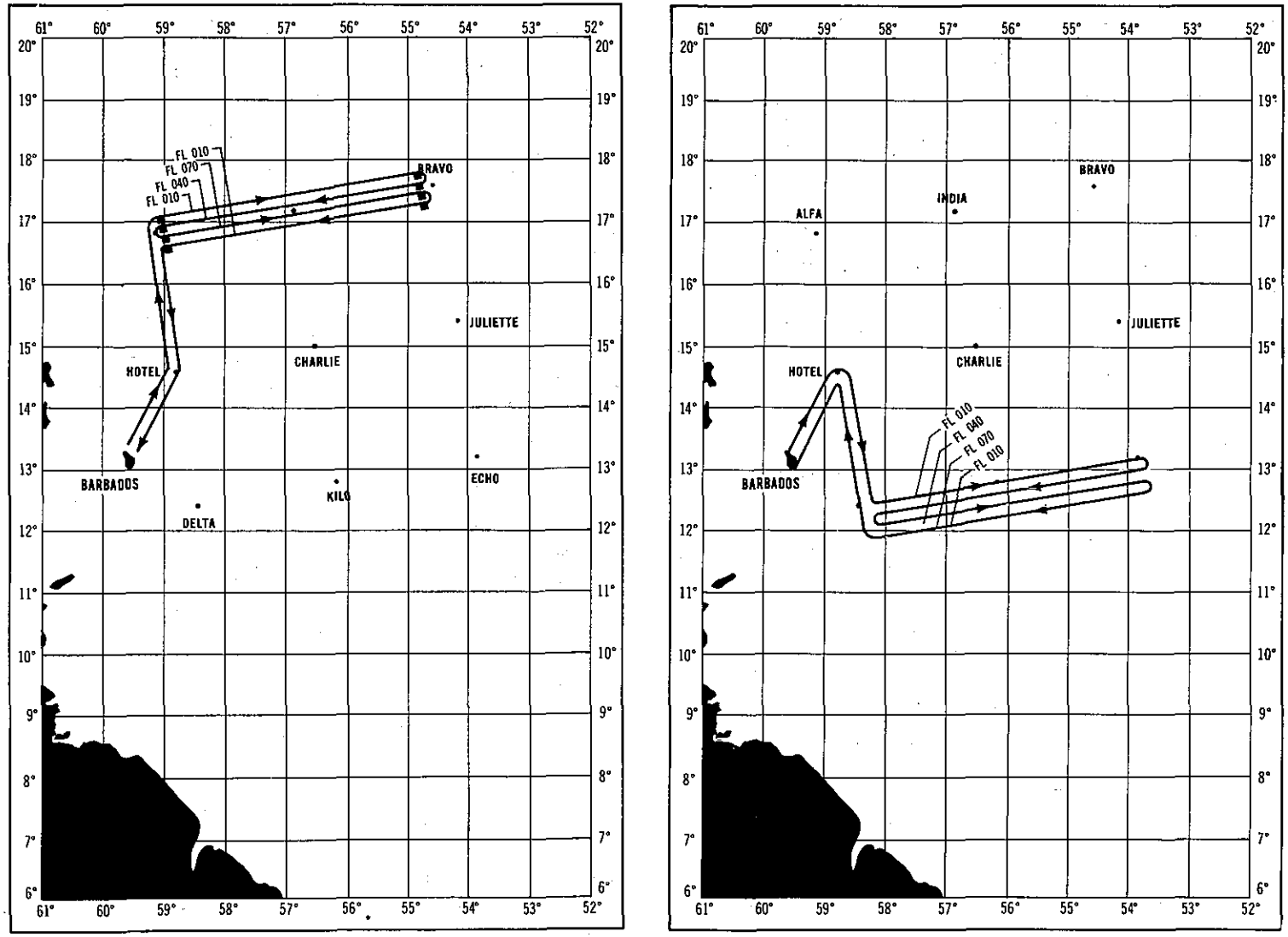

Figure 1.--Aircraft line integral flight pattern.

2.2 Rawinsonde Data

Rawinsonde data from the four ships positioned at the corners of the BOMEX square were used in this study. The orientation of the square was such that the two sides were roughly parallel to the climatological mean low-level flow from 080°. Launchings were made simultaneously from the four ships at 1 1/2-hr intervals beginning at midnight GMT, except for 0130 GMT, when there was no sounding. One set of data used in this study for comparison with the aircraft data was obtained with rawinsondes released, simultaneously, nearest in time to that at which the aircraft covered one flight leg at each level. For simplicity, the simultaneous releases will be referred to as "single release." The other set of data consisted of 6-hr averages obtained from four rawinsonde observations made 1 1/2 hr and 3 hr before and after the single release. The single-release data consisted of 30-mb averages centered at $p^* = 130$ mb and $p^* = 220$ mb and served as the basic data set corresponding to the aircraft data at the 1,300- and 2,300-m levels. At $p^* = 30$ mb, which corresponds to the aircraft data at the 300-m level, the data were not averaged vertically, because the winds below 30 mb were not reliably measured. From the 6-hr data set, values were computed for 50-mb slices for the two upper levels. Note that in these calculations, as in the study by Holland and Rasmusson (1973), a p^* coordinate system is used, where p^* is the position on the vertical axis in terms of pressure differential relative to sea level, i.e., $p^* = 0$ at sea level and 500 mb at the top of the BOMEX "box."

3. INTERCOMPARISON AND RESULTS

Of the two types of data sets used, each has its advantages and disadvantages, each to some degree complementing the other. The maximum frequency for the aircraft missions was one every 1 1/2 days. During each mission, sampling was done on the four flight levels in 7 hr. Rawinsondes, on the other hand, were released at 1 1/2-hr intervals daily. The aircraft, therefore, had the capability of high resolution in the horizontal, but their time and vertical resolution was limited. This was compensated for by the good vertical and time resolution of the rawinsondes, whose horizontal resolution was limited to the 500-km spacing between the ships.

3.1 Effect of Small-Scale Horizontal Eddies

The aircraft data made it possible to evaluate the spatial eddy contribution to the water-vapor flux divergence, of which the zonal component is shown in table 1. The last column in this table represents the eddy contribution that would remain if the linear trend along the flight leg were removed from the specific humidity and normal wind component. This contribution could not be measured by the BOMEX rawinsondes. As seen in table 1, there are only two cases, at 2,300 m on June 24 and June 30, 1969, in which the eddy contribution is as large as 10 percent of the total. This shows that under relatively undisturbed trade-wind flow during the 5 days examined here, the small-scale spatial eddies below the trade-wind inversion are either unimportant or cannot be measured by the aircraft system. A study by Holland and Acheson (1973) indicates that variability on scales of less than

Table 1.--Zonal contribution to the water-vapor flux divergences based on RFF aircraft data (10^{-5} $g.kg^{-1}$ s^{-1})

Date	Level (m)	Total	Eddy	Nonlinear eddy
June 22	300	46.0	-0.2	-0.2
	300	- 3.4	0.0	0.0
	1,300	-28.0	0.0	-0.2
	2,300	60.8	1.6	-1.2
June 24	300	60.6	-0.4	-0.2
	300	17.0	-0.4	-0.2
	1,300	8.8	-0.2	-0.4
	2,300	12.4	4.0	0.0
June 26	300	86.8	-0.6	0.2
	300	92.2	0.0	-0.2
	1,300	80.2	0.6	-0.2
	2,300	36.4	0.2	-0.2
June 29	300	13.6	-0.4	-0.6
	300	6.0	-0.4	-0.4
	1,300	77.2	-0.4	-0.4
	2,300	73.8	2.0	0.2
June 30	300			
	300	-31.2	0.0	0.0
	1,300	-28.2	-1.0	-0.6
	2,300	- 5.6	-0.6	0.8

20 km as measured by aircraft probably is noise. If the small-scale eddies were important, we would not expect the contributions to be coming from eddies of less than 20-km scale. The finding that horizontal eddies on scales of less than 500 km are of no importance is one of the significant results of this study of BOMEX aircraft data.

3.2 Spatial Wind Derivatives

As noted in the introduction, preliminary atmospheric budget analyses were presented by Holland and Rasmusson (1973). The major term in the water-vapor budget equation is, as they pointed out, the mean divergence term. $q\nabla\cdot\vec{V}$, rather than advection of moisture, $\vec{V}\cdot\nabla q$. Therefore, the accuracy with which the water-vapor flux divergence is computed depends heavily on the accuracy of the kinematic divergence measurements. In this section we shall examine several comparisons of wind derivatives, in terms of time and space, obtained from the various data sets. For purposes of these intercomparisons, the data were stratified into two groups, the 300-m level data forming the lower, and the 1,300- and 2,300-m data, the upper group.

3.2.1 Representativeness in Time

To establish the representativeness of the horizontal wind derivatives obtained from the rawinsonde single-release data, these data were compared with the 6-hr average values. Figure 2 shows comparison for $\partial u/\partial x$ and $\partial v/\partial y$ for both groups. The x and y axes have been rotated 10^{o} counterclockwise to coincide with the ship-array orientation. Each point on the scatter diagrams represents a spatial derivative as determined from wind measurements on two ships. To be noted here are the high correlation coefficients and the low rms differences for the $\partial u/\partial x$ comparisons, indicating less variability for short periods in the computed values of $\partial u/\partial x$. This high correlation between the u derivatives is very encouraging because it establishes some confidence in the single release as being quite representative of the 6-hr average. The lower correlation for $\partial v/\partial y$ cannot be readily interpreted, for it may be due either to noisier measurements or actual fluctuations over short periods. However, rms differences of 3×10^{-6} s^{-1} indicates that the single release is still a noisy measurement. This was to be expected, and was the reason for the frequent rawinsonde time sampling during BOMEX.

Table 2 shows the population means and standard deviations, as well as the rms differences, between the single-release and 6-hr average data. The mean divergence values show better agreement at upper levels, and also indicate that at these levels the sum of $\partial u/\partial x$ and $\partial v/\partial y$ is almost zero. The discrepancies between the means contribute much to the rms differences at lower levels.

3.2.2 Representativeness in Space

To examine the spatial uniformity of the wind derivatives, values of the same derivative quantity measured on opposite sides of the BOMEX array were compared. In all cases, for both upper and lower levels and for both aircraft

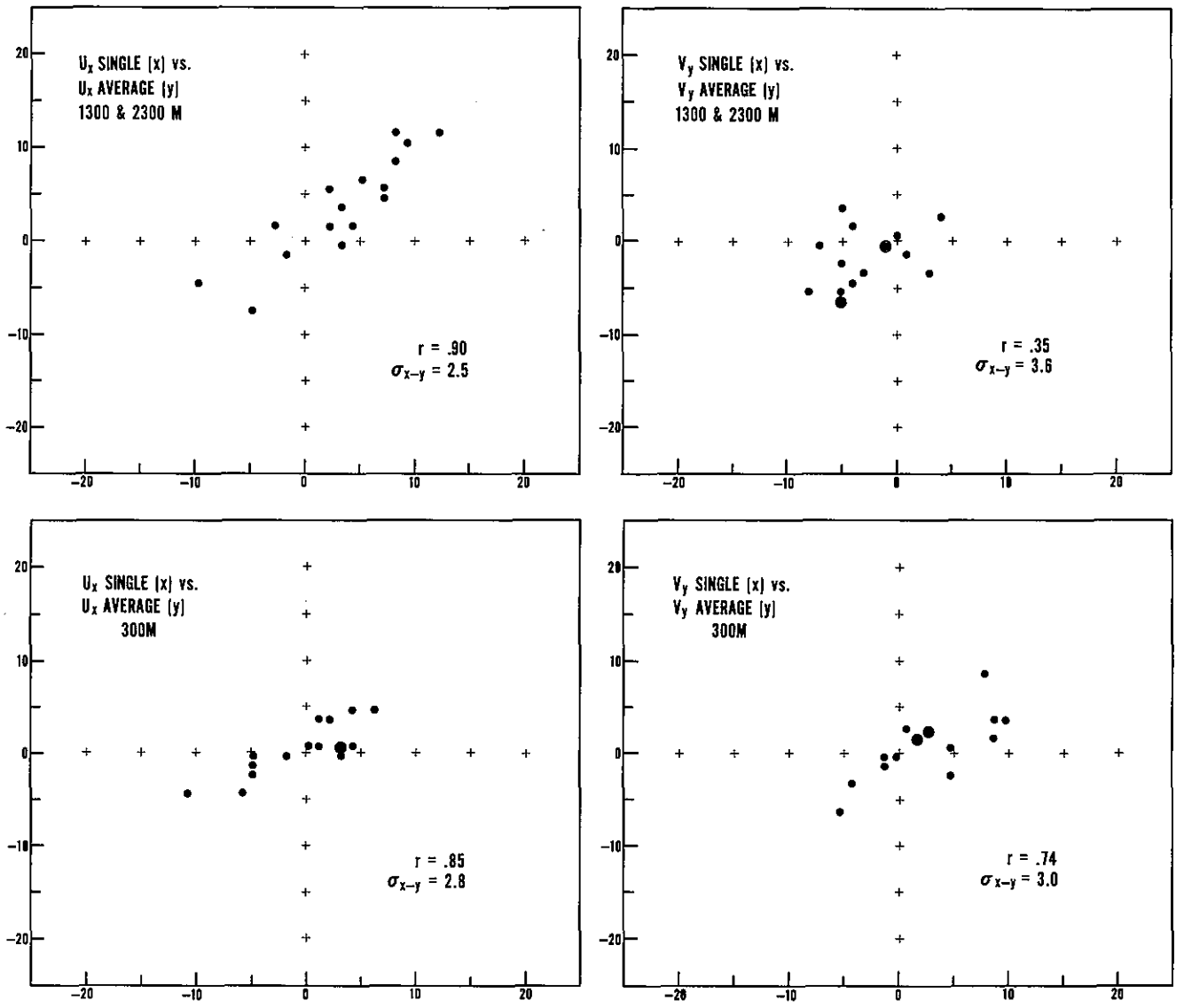

Figure 2.--Spatial wind derivatives. Rawinsonde single release vs. 6-hr average for $\partial u/\partial x$ (U_x) and $\partial v/\partial y$ (V_y). Units: 10^{-6} s^{-1}. In this figure, as in those that follow, r is the correlation coefficient, and σ_{x-y} is the rms difference between the variates.

Table 2.--Means, standard deviations, and rms differences for wind derivative comparisons

	∂u/∂x						∂v/∂y					
	Lower level			Upper level			Lower level			Upper level		
	Mean	σ	rms diff.	Mean	σ	rms diff.	Mean	σ	rms diff.	Mean	σ	rms diff.
Rawinsonde single release	-0.4	4.7	2.8	3.2	5.7	2.5	2.9	4.5	3.0	-2.9	3.4	3.6
Rawinsonde 6-hr average	+0.9	2.7		3.1	5.3		1.4	3.3		-2.7	2.9	
Rawinsonde single release across northern part of array Rawinsonde single release across southern part of array			6.4			9.4						
Rawinsonde single release across eastern part of array Rawinsonde single release across western part of array									5.5			4.3
Rawinsonde 6-hr average across northern part of array	-0.1	1.7	3.3	4.4	4.4	9.0						
Rawinsonde 6-hr average across southern part of array	-0.3	3.6		1.7	5.8							
Rawinsonde 6-hr average across eastern part of array							3.0	2.2	4.6	-2.4	2.5	3.6
Rawinsonde 6-hr average across western part of array							2.9	2.5		-3.3	2.4	
Aircraft trend method across northern part of array	0.9	3.4	4.6	3.0	4.9	8.5						
Aircraft trend method across southern part of array	0.5	3.2		1.1	5.8							
Aircraft trend method across eastern part of array							4.8	2.9	8.5	-1.2	3.5	5.4
Aircraft trend method across western part of array							-3.2	6.7		-4.9	3.9	

and rawinsondes (single release and 6-hr average), the correlation coefficient was found not to differ significantly from zero at the 5-percent level. This is a surprising result, and indicates that the time variations of a single measurement of a spatial derivative along a 500-km path cannot be used to represent the variations of the same quantity at a lateral distance of 500-km on the time scale of 1 1/2 hr to 2 days.

Rawinsonde mean values are almost the same at lower levels, but differ substantially at upper levels. Aircraft mean values are comparable only for low-level $\partial u/\partial x$ measurements.

3.2.3 Aircraft Trend Method vs. Rawinsondes

Divergence estimates can be obtained from aircraft data by two methods. The line integral technique, or boundary method, involves measuring the outward normal component of the wind along the perimeter of an area in order to obtain the area-average divergence. This was the method used in the Indian Ocean Experiment (Fleagle et al. 1967). Aircraft can also, however, measure the spatial wind derivatives parallel to the flight track. Holland (1971) has suggested a "trend" method for obtaining divergence estimates from such measurements. By this method, a least-squares linear trend is fitted to the data along a flight path. The large-scale spatial derivatives of the wind in the direction of flight can then be determined, and values of divergence can, in turn, be obtained by combining the derivatives from the two intersecting, perpendicular flight tracks.

Spatial derivatives computed by the trend method along each side of the BOMEX "box" were compared for purposes of this study with data from two rawinsonde stations at the ends of the corresponding sides. The results are shown in figure 3, where each point represents a spatial derivative as determined from the two stations and a single aircraft. Note the improvement in the comparisons when the rawinsonde 6-hr averages are used instead of the single-release values.

By averaging the spatial derivatives on opposite sides of the array, we form an estimate of the area average of that spatial derivative. Each value then represents a spatial derivative as determined from four ship stations or two aircraft. The results of this comparison and the comparisons to be discussed in the sections that follow are given in tables 3 and 4. Note the high correlation values and low rms differences for $\partial u/\partial x$ at the upper levels, a finding that establishes confidence in the use of endpoint values to estimate spatial derivatives. The poor correlation at low levels must be partly due to the small-scale time variability that yielded lower correlation coefficients in the earlier comparison between rawinsonde single-release and 6-hr average data.

3.2.4 Aircraft Boundary Method vs. Rawinsondes

Results of comparison between wind derivatives computed by the aircraft boundary method and from rawinsonde 6-hr averages for the four ship stations are shown in figure 4 and table 3. Despite the discouragingly low correlation coefficients, the rms differences lie between 1×10^{-6} s^{-1} and 4×10^{-6} s^{-1}.

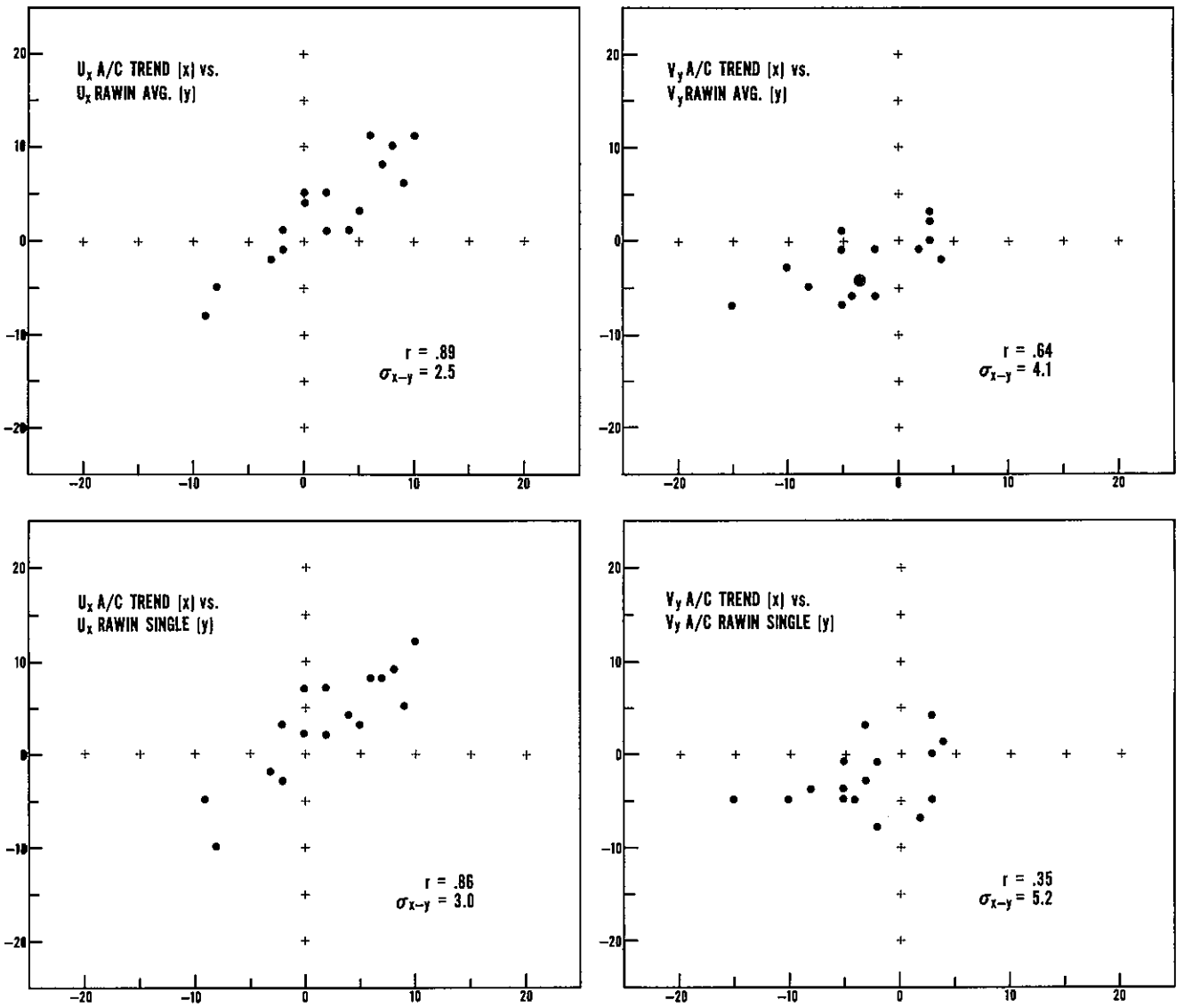

Figure 3.--Spatial wind derivatives. Rawinsonde single release and 6-hr average vs. aircraft trend method at 1,300 and 2,300 m for $\partial u/\partial x$ (U_x) and $\partial v/\partial y$ (V_y). Units: 10^{-6} s^{-1}.

Table 3.--Comparisons of zonal and meridional contributions to the horizontal velocity divergence (10^{-6} s^{-1})

	Number of comparisons	300-m level ∂u/∂x	300-m level ∂v/∂y	1,300- and 2,300-m level ∂u/∂x	1,300- and 2,300-m level ∂v/∂y
Aircraft trend vs. rawinsondes	8				
rms difference		3.1	1.6	1.0	2.2
mean difference (trend minus rawinsondes)		1.3	-2.2*	-1.6*	-0.3
Aircraft boundary vs. rawinsondes	8				
rms difference		2.3	3.9	1.2	2.8
mean difference (boundary minus rawinsondes)		1.6	0.0	-1.3*	-1.4
Aircraft trend vs. boundary	10				
rms difference		2.4	4.1	3.7	3.2
mean difference (trend minus boundary)		1.2	-1.4	-1.7	0.6

Note: The rms difference is not the same as in the diagrams, because in the values given here the mean difference has been removed. Values noted by an asterisk are those indicated by the Student t test to be exceeded in magnitude less than 10 percent of the time.

Table 4.--Comparisons of rawinsonde and aircraft horizontal velocity divergence and water-vapor flux divergence

	RFF	Navy	Trend	Rawinsondes vs. Boundary	A/C average*
Lower-level horizontal velocity divergence					
Number of comparisons	8	7	7	7	7
$\sigma_{rawinsondes}$ (10^{-6} s^{-1})	2.6	2.4	2.4	2.4	2.4
$\sigma_{aircraft}$ (10^{-6} s^{-1})	4.4	4.1	2.2	5.3	3.1
Correlation coefficient	0.36	0.24	0.27	0.44	0.47
Mean difference (rawinsondes minus A/C; 10^{-6} s^{-1})	0.6	-1.3	1.0	-2.2	-0.6
rms difference (10^{-6} s^{-1})	4.2	4.3	2.8	4.8	2.9
Lower-level water-vapor flux divergence					
Number of comparisons	8	7	7	7	7
$\sigma_{rawinsondes}$ (10^{-5} g kg^{-1} s^{-1})	4.5	4.4	4.4	4.4	4.4
$\sigma_{aircraft}$ (10^{-5} g kg^{-1} s^{-1})	7.2	6.8	3.5	9.0	5.2
Correlation coefficient	0.34	0.20	0.24	0.38	0.41
Mean difference (rawinsondes minus A/C; 10^{-5} g kg^{-1} s^{-1})	1.2	-0.3	3.6	-2.3	0.2
rms difference (10^{-5} g kg^{-1} s^{-1})	7.1	7.3	4.9	8.4	5.3

Table 4.--Comparisons of rawinsonde and aircraft horizontal velocity divergence and water-vapor flux divergence (continued)

	RFF	Navy	Rawinsondes vs. Trend	Rawinsondes vs. Boundary	A/C average*
Upper-level horizontal velocity divergence					
Number of comparisons	8	8	8	8	8
$\sigma_{rawinsondes}$ (10^{-6} s^{-1})	1.7	1.7	1.7	1.7	1.7
$\sigma_{aircraft}$ (10^{-6} s^{-1})	2.6	4.5	4.0	3.0	3.0
Correlation coefficient	0.72	0.33	0.55	0.41	0.57
Mean difference (rawinsondes minus A/C; 10^{-6} s^{-1})	1.5	2.9	1.8	2.7	2.2
rms difference (10^{-6} s^{-1})	1.9	4.3	3.4	2.8	2.5
Upper-level water-vapor flux divergence					
Number of comparisons	8	8	8	8	8
$\sigma_{rawinsondes}$ (10^{-5} g kg^{-1} s^{-1})	2.4	2.4	2.4	2.4	2.4
$\sigma_{aircraft}$ (10^{-5} g kg^{-1} s^{-1})	3.6	4.9	5.2	4.4	3.9
Correlation coefficient	0.64	0.34	0.38	0.46	0.52
Mean difference (rawinsondes minus A/C; 10^{-5} g kg^{-1} s^{-1})	0.8	5.2	3.9	2.4	3.0
rms difference (10^{-5} g kg^{-1} s^{-1})	2.8	4.6	4.8	3.9	3.4

* Average of the trend and boundary methods.

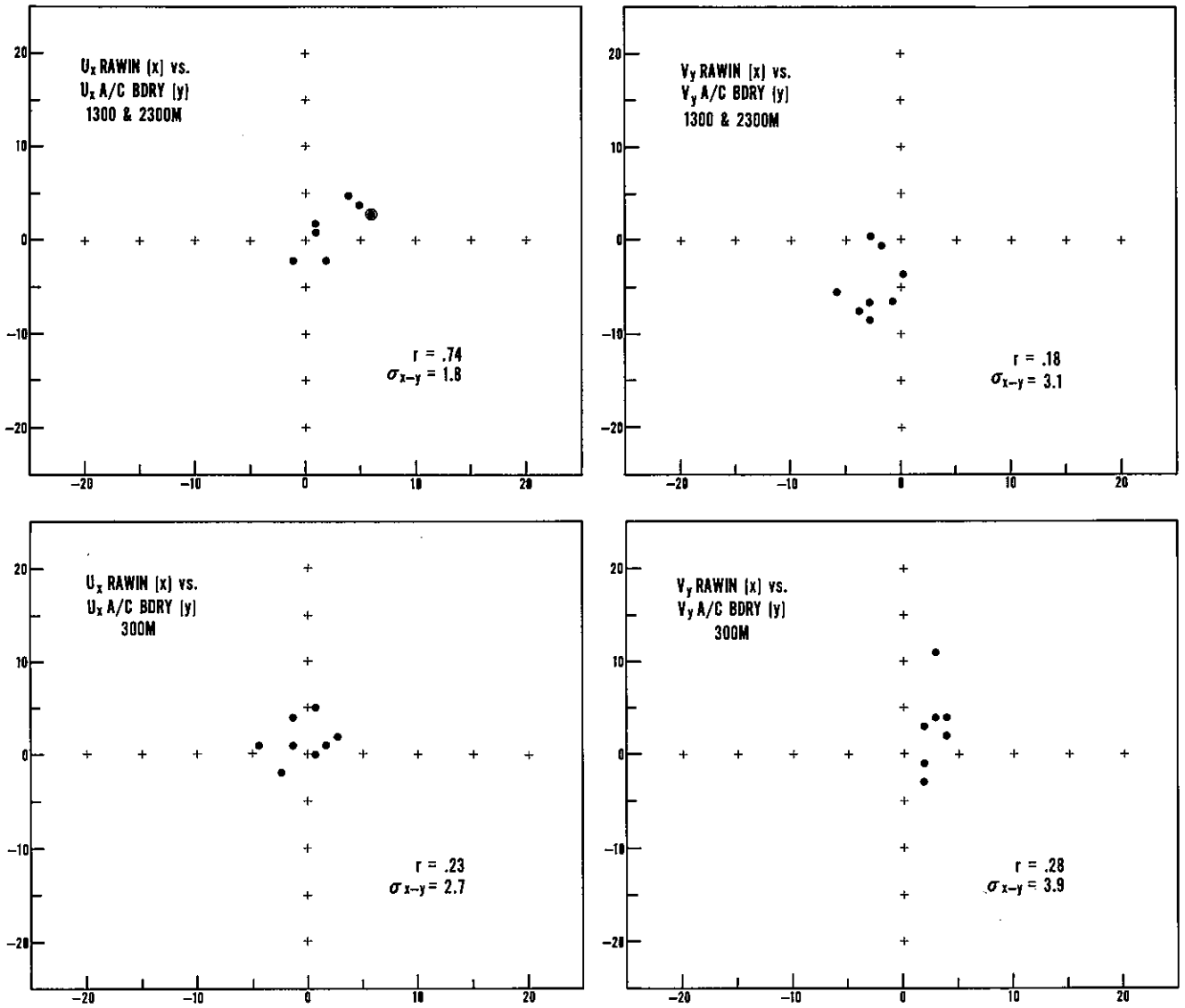

Figure 4.--Spatial wind derivatives. Rawinsonde 6-hr average vs. aircraft boundary method for $\partial u/\partial x$ (U_x) and $\partial v/\partial y$ (V_y). Units: 10^{-6} s^{-1}.

3.2.5 Aircraft Trend vs. Aircraft Boundary Method

The comparisons here involve not only two methods, but also two aircraft measuring systems. As noted in section 2.1, on the Navy aircraft operating on the north and south sides of the BOMEX array, manual recording systems were used. Both $\partial u/\partial x$, determined by the trend method, and $\partial v/\partial y$, obtained by the boundary method, are therefore derived from hand-tabluated data. Although the correlation coefficients are generally low (fig. 5), the rms differences (table 3) indicate better agreement at upper levels. Exclusion of the single bad point on the diagram for $\partial u/\partial x$ at upper levels would lower the rms difference for that comparison from 4.1×10^{-6} s^{-1} to 1.6×10^{-6} s^{-1}.

3.3 Water-Vapor Flux Divergences

Figure 6 shows aircraft vs. rawinsonde comparisons for the zonal and meridional contributions to $\nabla \cdot q\vec{V}$, the total vapor flux divergence. The rms difference for the rawinsonde zonal vs. aircraft trend zonal comparison is larger than we would have expected, considering the low rms values for the divergence comparisons between the two measurement systems.

By combining the zonal and meridional contributions, we obtain the total water-vapor flux divergence. Among the several comparisons of the various systems shown in figure 7, note that the best agreement is obtained for comparisons involving RFF aircraft data. The diagram in the lower right of this figure contains two sets of data. The x's represent Navy aircraft data to which airspeed and drift-angle corrections have been applied by use of calibration box data. Even after such corrections, however, biases still remain. These can be eliminated by use of data collected on the intercomparison legs. Applying this second set of corrections, as the diagram in figure 7 shows, increases the correlation coefficient from 0.75 to 0.93 and reduces the rms difference from 3.4×10^{-5} $g \cdot kg^{-1}$ s^{-1} to 2.4×10^{-5} $g \cdot kg^{-1}$ s^{-1}. This illustrates the importance of using data from the intercomparison legs for calibration purposes.

3.4 Sea-Surface Evaporation

The next step is to compute the sea-surface evaporation rate from the calculated water-vapor flux divergence. To do so, several assumptions have to be made:

(1) The vertical eddy flux of water vapor is negligible at 2,300 m, the upper part of the trade inversion. The rawinsonde budget computations for the same period showed approximately 25 percent of the surface value at this level (Rasmusson 1971).

(2) There is no net condensation or evaporation within the BOMEX "box."

(3) The data at the aircraft levels are valid for finite thicknesses of the atmosphere.

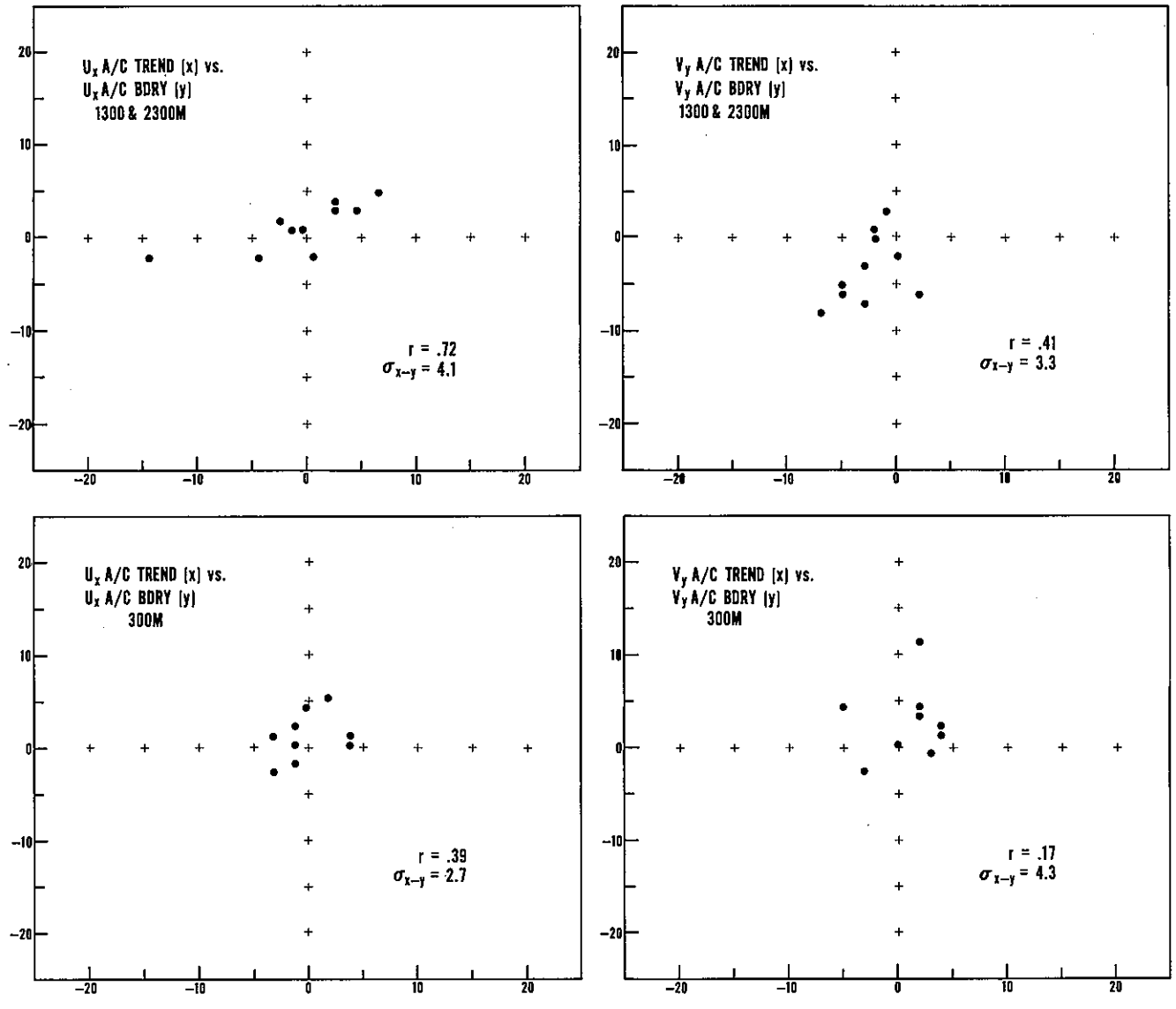

Figure 5.--Spatial wind derivatives. Aircraft trend vs. aircraft boundary method for $\partial u/\partial x$ (U_x) and $\partial v/\partial y$ (V_y). Units: 10^{-6} s^{-1}.

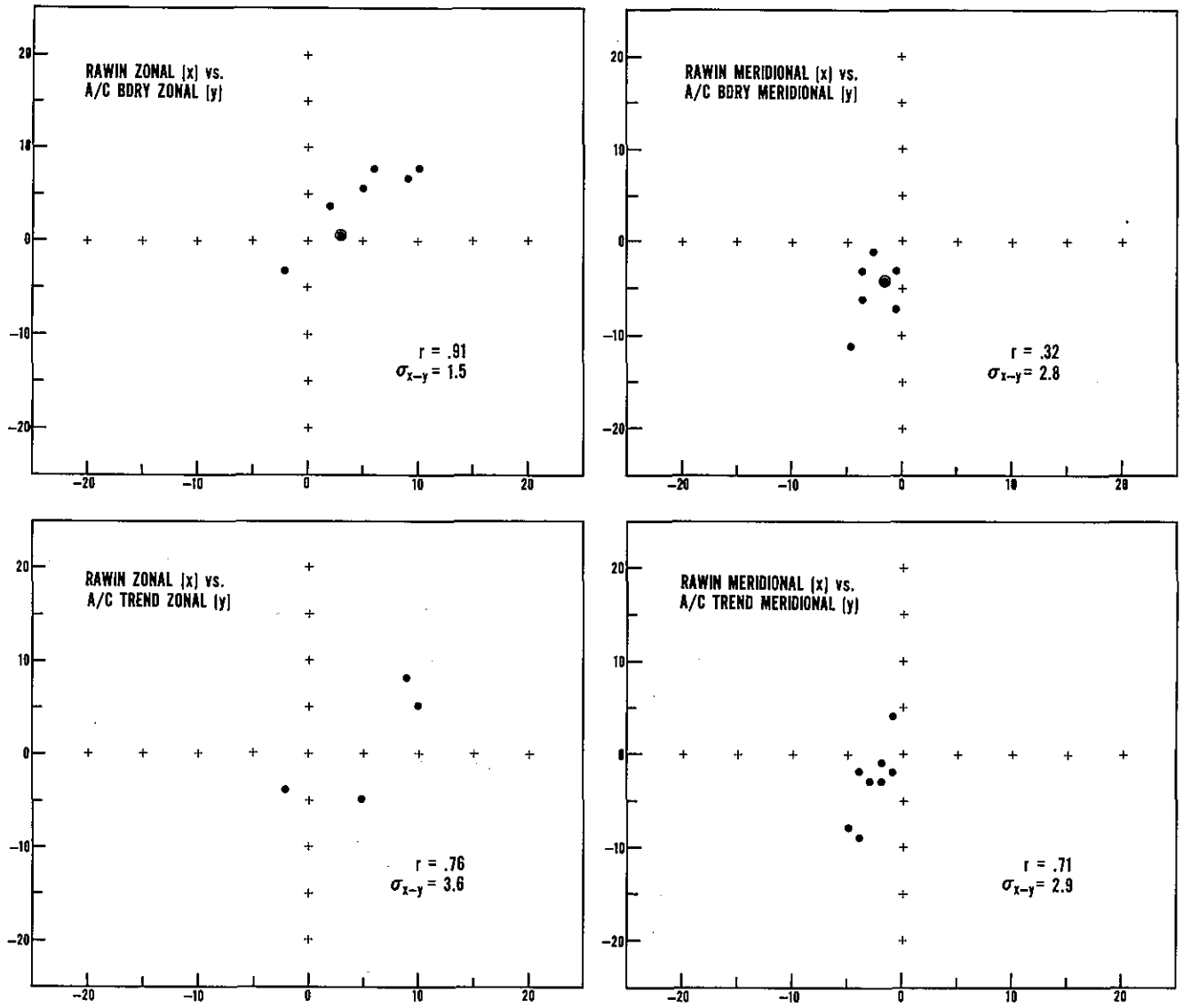

Figure 6.--Spatial water-vapor flux derivatives. Rawinsonde 6-hr average vs. aircraft trend and boundary methods at 1,300 and 2,300 m for the zonal and meridional parts of the horizontal water-vapor flux divergence. Units: 10^{-5} $g \cdot kg^{-1}$ s^{-1}.

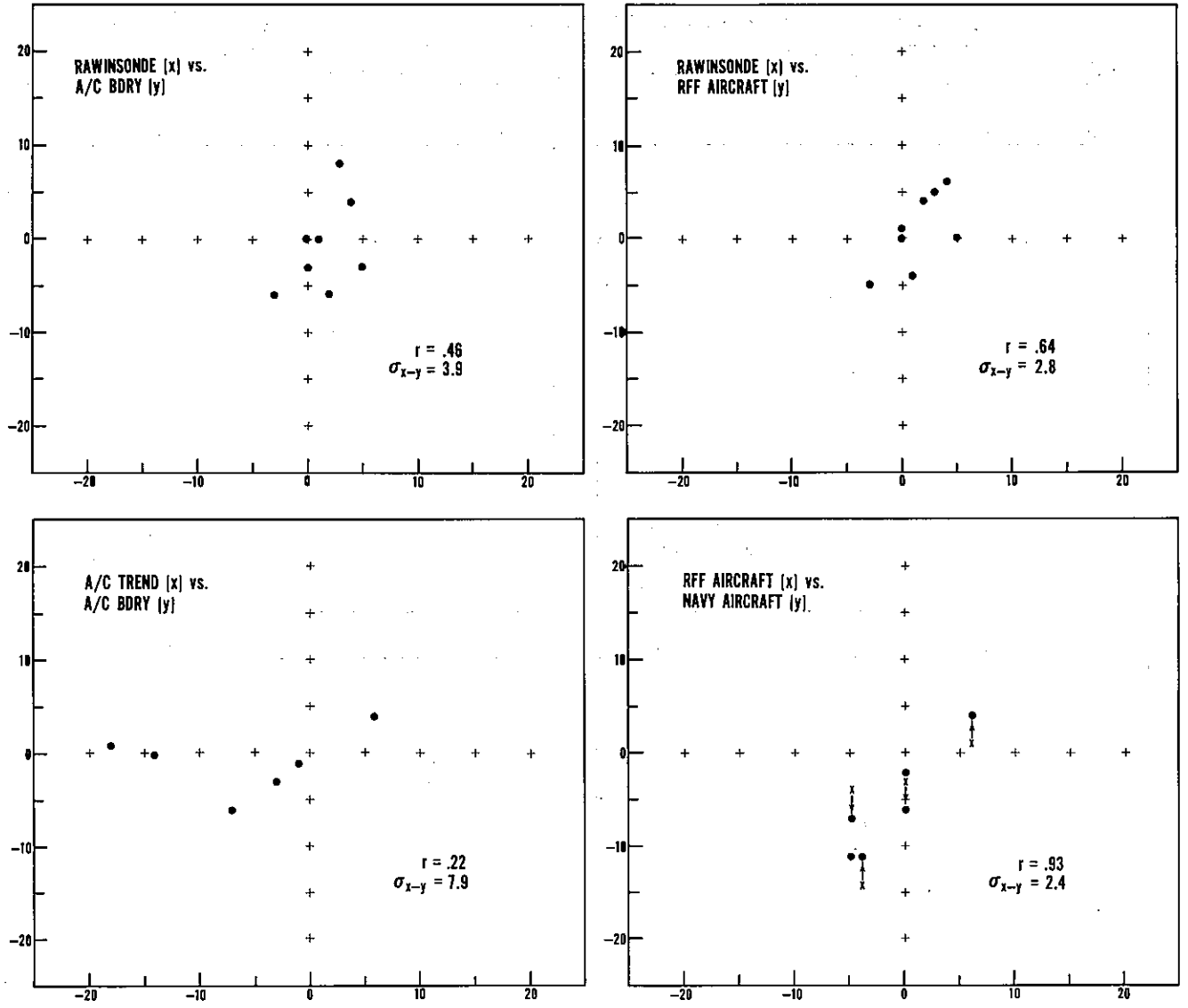

Figure 7.--Spatial water-vapor flux derivatives. Several comparisons based on rawinsonde 6-hr averages and the various aircraft systems and methods at 1,300 and 2,300 m for the horizontal water-vapor flux divergence. Units: 10^{-5} g·kg^{-1} s^{-1}.

(4) Steady state is assumed for the upper two levels, since information about the time rate of change is available from the aircraft data only at 300 m.

Although the average obtained for three missions by the boundary method yielded a reasonable estimate of evaporation (5 mm·day^{-1}), the computed values for individual missions appear either too low (2 mm·day^{-1}) or too high (11 mm·day^{-1}).

The unrealistic value of -2 mm day^{-1} (table 5) computed from the June 22 RFF aircraft data is the result of large mass convergence measurement by the trend method by a single aircraft along one of the 300-m flight legs. This value dominates the calculation, giving an unrealistic kinematic upward vertical velocity at the top of the lowest layer. The evaporation rates computed from 24-hr rawinsonde averages are 12, 8, 4, and 7 mm day^{-1} for June 22 to June 25.

Table 5.--Evaporation rate estimates from aircraft data (mm·day^{-1})

	Aircraft boundary method	RFF aircraft
June 22, day	2	-2
June 23-24, night	2	6
June 25-26, night	11	9

4. SUMMARY AND CONCLUSIONS

Estimates of the water-vapor flux divergence were obtained by the line integral technique from BOMEX aircraft data. The zonal part was measured by the RFF aircraft on several undisturbed days. Typical values for the 300-m level lie between 10^{-3} and 10^{-4} g·kg^{-1} s^{-1}, the eddy contribution being less than 10^{-5} g·kg^{-1} s^{-1}.

Typical values of the horizontal velocity divergence are +1 to +3 x 10^{-6} s^{-1}, the divergence being somewhat higher at 1,300 m and near zero at 2,300 m. Population standard deviations range from 2 x 10^{-6} s^{-1} to 7 x 10^{-6} s^{-1}, and are larger than the mean in most cases.

For comparison of the measuring systems, the rms differences and correlation coefficients were considered useful, since the large population sigmas may represent natural variability. The rms differences for the divergence measurements ranged from 2 x 10^{-6} s^{-1} to 5 x 10^{-6} s^{-1}.

The high correlation coefficients for the $\partial u/\partial x$ measurements (0.9) indicates that the aircraft and rawinsondes were measuring the same atmospheric property. The $\partial v/\partial y$ measurements by different methods were uncorrelated.

The total water-vapor flux divergence was computed for the various systems, and the low correlation, as well as the large differences in the means, is discouraging.

A few conclusions can be drawn from the comparisons made in this study:

(1) The contribution of subgrid-scale eddies to the horizontal water-vapor flux divergence is unimportant beneath the trade-wind inversion during relatively undisturbed weather conditions.

(2) The high correlation between the u derivatives based on rawinsonde single release and 6-hr average, establishing the single release as representative of the 6-hr average, is encouraging. The rms difference of 3×10^{-6} s^{-1}, however, indicates that the single release is still a noisy measurement.

(3) The large correlation coefficients and low rms values in the comparison between the aircraft trend method and rawinsondes for the u derivatives at the upper levels gives confidence in the use of endpoint rawinsonde data to estimate spatial derivatives.

(4) The wind derivatives across the BOMEX array showed surprisingly large variability, but in spite of these large variations the rms differences in the comparisons of the aircraft boundary method vs. rawinsondes and the aircraft boundary vs. aircraft trend method were found to be low at the upper levels. This suggests that the derivatives change almost linearly across the array at these levels, which means that the sampling problem is not as great as thought at first. It also confirms previous hypotheses concerning the scales of motion in the trade-wind region. Malkus (1956) described this region as being characterized by predominantly small-scale motions at lower levels and by large-scale motions above the trade-wind inversion. The aircraft data studied here indicate that the variability across the array is greater at the upper levels for the x and y derivatives of both u and v, which suggests significant variations with scales of at least 500 km, the length of each side of the BOMEX square.

(5) The rms values for the aircraft data sets are lower than for the rawinsonde single-release data, but the rms differences for the 6-hr 50-mb average rawinsonde data are about the same as for the RFF aircraft. We can interpret this loosely to mean that the accuracy of 500-km horizontal divergence measurements on a single four-aircraft mission is comparable to the accuracy of the 6-hr 50-mb rawinsonde averages.

ACKNOWLEDGMENTS

Many people contributed to the processing of the data used in this study. I am particularly grateful to Billy M. Lewis, Donald T. Acheson, and Peter Pytlowany for their efforts in processing the aircraft data, and to Eugene M. Rasmusson and Thomas Carpenter, who played an important role in the rawinsonde data reduction.

REFERENCES

BOMAP Office, BOMEX Field Observations and Basic Data Inventory, National Oceanic and Atmospheric Administration, U.S. Department of Commerce, Rockville, Md., 1971, pp. 24-47.

Fleagle, R.G., F.I. Badgley, and Y. Hsueh, "Calculation of Turbulent Fluxes by Integral Methods," Journal of Atmospheric Sciences, Vol. 24, No. 4, 1967, pp. 356-373.

Holland, J.Z., "Preliminary Report on the BOMEX Sea-Air Interaction Program," Bulletin of the American Meteorological Society, Vol. 51, No. 9, 1970, pp. 809-820.

Holland, J.Z., "Interim Report on Results From the BOMEX Core Experiment," BOMEX Bulletin, No. 10, BOMAP Office, National Oceanic and Atmospheric Administration, U.S. Department of Commerce, Rockville, Md., 1971, pp. 31-43.

Holland, J.Z., and D.T. Acheson, "Observation System Intercomparison - Examples From BOMEX, "IEEE Transactions on Geoscience Electronics, Vol. GE-11, No. 2, 1973, pp. 101-109.

Holland, J.Z., and E.M. Rasmusson, "Measurements of the Atmospheric Mass, Energy, and Momentum Budgets Over a 500-Kilometer Square of Tropical Ocean," Monthly Weather Review, Vol. 10, No. 1, 1973, pp. 44-55.

Malkus, Joanne S., "On the Maintenance of the Trade Winds, Tellus, Vol. VIII, 1956, pp. 335-350.

Rasmusson, E.M., "Mass, Momentum, and Energy Budget Equations for BOMAP Computations," NOAA Technical Memorandum ERL BOMAP-3, BOMAP Office, National Oceanic and Atmospheric Administration, U.S. Department of Commerce, Rockville, Md., 1971, 32 pp.

Reeves, R.W., "Preliminary Velocity Divergence Computations for BOMEX Volume Based on Aircraft Winds," NOAA Technical Memorandum ERL BOMAP-5, BOMAP Office, National Oceanic and Atmospheric Administration, U.S. Department of Commerce, Rockville, Md., 1971, 21 pp.

APPENDIX

Computation of Water-Vapor Flux Divergence and Sea-Surface Evaporation

The water-vapor conservation equation for a parcel of air can be written

$$\frac{dq}{dt} = e - c \ , \tag{A-1}$$

where q is the specific humidity, e is the evaporation, and c is the condensation. Expanding the substantial derivative, $\frac{dq}{dt}$, we have

$$\frac{dq}{dt} = \frac{\partial q}{\partial t} + \mathbb{V}\cdot\nabla q + \omega^* \frac{\partial q}{\partial p^*} \ , \tag{A-2}$$

where the vertical coordinate, p*, is given by $p^*(z) = p\ (sfc) - p(z)$, and $\omega^* \equiv \frac{dp^*}{dt}$.

Using the mass continuity equation,

$$\nabla\cdot\mathbb{V} + \frac{\partial \omega^*}{\partial p^*} = 0 \ ,$$

we can write eq (A-1) in flux form as

$$\frac{\partial q}{\partial t} + \nabla\cdot q\ \mathbb{V} + \frac{\partial}{\partial p^*}(q\omega^*) = e - c \ . \tag{A-3}$$

Averaging eq (A-3) over area A gives

$$\frac{\partial \tilde{q}}{\partial t} + \widetilde{\nabla\cdot q\ \mathbb{V}} + \frac{\partial}{\partial p^*}\widetilde{(q\omega^*)} = \tilde{e} - \tilde{c} \ , \tag{A-4}$$

where $\widetilde{(\quad)} = \frac{1}{A}\int (\quad)\, dA.$

In addition, we can write each quantity as an area average plus a deviation from the area average using the following notation:

$$(\quad) = \widetilde{(\quad)} + (\quad)''$$

The third term on the left side of eq (A-4) can then be rewritten

$$\frac{\partial}{\partial p^*}\widetilde{(q\omega^*)} = \frac{\partial}{\partial p^*}(\tilde{q}\ \tilde{\omega}^*) + \frac{\partial}{\partial p^*}\widetilde{(q''\omega^{*''})} ,$$

where the term $\frac{\partial}{\partial p^*}\widetilde{(q''\omega^{*''})}$ is the vertical gradient of the subgrid-scale water-vapor flux.

Vertical integration of eq (A-4) from the sea surface ($p^* = 0$) to some level p_T^* gives

$$\int_0^{p_T^*} \frac{\partial \tilde{q}}{\partial t}\, dp^* + \int_0^{p_T^*} \widetilde{\nabla\cdot q\ \mathbb{V}}\, dp^* + (\tilde{q}\ \tilde{\omega}^*)_{p_T^*} - (\tilde{q}\ \tilde{\omega}^*)_0$$

$$+ \widetilde{(q''\omega^{*''})}_{p_T^*} - \widetilde{(q''\omega^{*''})}_0 = \int_0^{p_T^*} (\tilde{e} - \tilde{c})\, dp^* . \qquad \text{(A-5)}$$

Equation (A-5) can be further simplified by noting that $\tilde{\omega}_o^* = 0$, and that the subgrid-scale water-vapor flux, $\widetilde{(q''\omega^{*''})}$, is the sea-surface evaporation, $\tilde{E}$, in the limiting case $p^* \to 0$. We also make the assumption that under undisturbed conditions nonprecipitating clouds are being created and dissipated at the same rate. Thus,

$$\int_0^{p_T^*} (\tilde{e} - \tilde{c})\, dp^* = 0,$$

and eq (A-5) becomes

$$\int_0^{p_T^*} \frac{\partial \tilde{q}}{\partial t}\, dp^* + \int_0^{p_T^*} \widetilde{\nabla\cdot q\ \mathbb{V}}\, dp^* + (\tilde{q}\ \tilde{\omega}^*)_{p_T^*} + \widetilde{(q''\omega^{*''})}_{p_T^*} = \tilde{E} \qquad \text{(A-6)}$$

Using the divergence theorem, we can transform the second term on the left side from an area integral to a line integral,

$$\widetilde{\nabla\cdot q\ \mathbb{V}} = \frac{1}{A}\oint_\Gamma qV_n\, d\Gamma ,$$

where the integration on the right side is performed around the perimeter of the area, Γ, and V_n is the component of the wind normal to the perimeter.

Since the BOMEX area was a square, an averaging process for each side, i, can be defined as

$$\overline{(\quad)}_i = \frac{1}{L}\int (\quad)_i dL \ ,$$

where L is the length of a side. Note that $L = \frac{\Gamma}{4}$, and $A = L^2$. Then,

$$\frac{1}{A}\oint_\Gamma q\, V_n\, d\Gamma = \frac{4}{L}\sum_{i=1}^{4}\overline{(qV_n)}_i \ . \qquad \text{(A-7)}$$

Thus quantities for a side of the array can also be written as the sum of the side average value plus a local deviation:

$$(\quad)_i = \overline{(\quad)}_i + (\quad)'_i \ .$$

Equation (A-7) then becomes

$$\frac{1}{A}\oint_\Gamma q\, V_n\, d\Gamma = \frac{4}{L}\sum_{i=1}^{4}[\overline{(q)}_i\overline{(V_n)}_i + \overline{(q'V_n')}_i] \ .$$

The second term on the right is the horizontal subgrid-scale water-vapor flux, part of which is represented by the contribution of the linear trends in V_n and q along the side. This contribution to the subgrid-scale flux was estimated from the rawinsonde data. The remaining part results from correlations of q and V_n arising from smaller scale variations, and was estimated from 1-s aircraft measurements along the side.

After these substitutions, the final equation is written

$$\int_0^{p_T^*}\frac{\partial \tilde{q}}{\partial t}\,dp^* + \int_0^{p_T^*}\frac{4L}{A}\sum_{i=1}^{4}[\overline{(q)}_i\,\overline{(V_n)}_i + \overline{(q'V_n')}_i]dp^*$$

$$+ \tilde{(q}\ \tilde{\omega^*)}_{p_T^*} + \tilde{(q''\,\omega^{*\prime\prime})}_{p_T^*} = E \ . \qquad \text{(A-8)}$$

Estimates of the sea-surface evaporation, $\tilde{E}$, were obtained by evaluating the left side of eq (A-8) based on data at several levels, under the assumption that the data at these levels apply to layers of finite thickness. The vertical integration is then approximated by a summation over the layers to a height p_T^*, where the subgrid-scale flux $(q''\omega^{*\prime\prime})_{p_T^*}$ is assumed negligible.